ARTICLE NO. 79-303R

J80-044

Calculation of Separated Turbulent Flows on Axisymmetric Afterbodies Including Exhaust Plume Effects

20007

Gary D. Kuhn*
Nielsen Engineering & Research, Inc., Mountain View, Calif.

A calculative method is presented for turbulent boundary-layer, inviscid flow interactions for axisymmetric configurations of the type used for isolated nozzle afterbody models. The method is applicable to flows with subsonic freestreams, including slightly supercritical flows, and to bodies with high-pressure exhaust plumes or solid plume simulators. Integral boundary-layer and plume entrainment methods are coupled iteratively with a finite-difference inviscid flow method through a boundary-layer plume displacement thickness. Results are presented which indicate that the procedure provides an accurate engineering prediction method for boattail flowfield with moderately underexpanded exhaust flows and for bodies with solid plume simulators.

Nomenclature

A_{nj} = coefficients, Eqs. (16), (18), and (28)
B_n = term, Eqs. (16), (18), and (32)
C = $\mu_w T_{e0}/\mu_{e0} T_w$
C_f = skin-friction coefficient
D = maximum body diameter
H_i = transformed shape factor, Eq. (19)
K = entrainment fraction, Eqs. (22) and (23)
L = reference length
M = Mach number
m = $[(\gamma-1)/2]M^2$
p = pressure
r = radius
S = $T_t/T_{te}-1$
S_n, S_s = functional forms of S defined in Eqs. (24-26)
s = root-mean-square error, Eq. (2)
T = temperature
t = transverse curvature factor in Eq. (12), $2L/r_w^2$
U, V = transformed X, Y velocity components
U_β = wake velocity defined in Eq. (13)
U_τ = friction velocity, Eq. (14)
u, v = x, r velocity components
u_n, u_s = functional forms of u defined in Eq. (22)
X, Y = transformed coordinates
x, y = physical coordinates defined in Fig. 3
x_s = location of separation point, Fig. 1
x_p = location of minimum velocity, Fig. 4
Y^+ = transformed coordinate [Eq. (15)]
$\bar{y}$ = $\int_0^y (r/L)\,dy$
β = eddy viscosity factor, $\tau/\mu(\partial u/\partial y)$
γ = ratio of specific heats
δ_i = transformed boundary-layer thickness
δ^* = displacement thickness
θ_s = half-angle of conical displacement surface
μ = molecular viscosity
ν = μ/ρ
ρ = density
τ = shear stress

Subscripts

0 = undisturbed freestream
c = inviscid core of exhaust jet
e = boundary-layer edge
I = inviscid flow
j = conditions in exhaust nozzle
t = stagnation conditions
V = viscous flow
w = conditions on a solid surface or at the inviscid jet boundary
$(\ )_x$ = differentiation with respect to x

Presented as Paper 79-0303 at the AIAA 17th Aerospace Sciences Meeting, New Orleans, La., Jan. 15-17, 1979; submitted Feb. 1, 1979; revision received July 17, 1979.

Index category: Jets, Wakes, and Viscid-Inviscid Flow Interactions.

*Senior Research Engineer. Member AIAA.

Introduction

ONE of the critical areas in the design of both aircraft and missiles is the interaction between propulsive jets and the external flow over the aerodynamic shapes from which they issue. Such flows are dominated by viscous effects such as boundary-layer separation and jet exhaust plume entrainment. The drag created by these effects can be a significant fraction of the total vehicle drag. Existing analytical attempts to predict these flows generally use the technique of dividing the flowfield into a number of analytical regions. Included are an inviscid external flow, an inviscid jet plume, and a viscous region which includes boundary layers on the afterbody boattail and inside the nozzle and a mixing layer between the jet and the external flow. Methods for calculating the entire flowfield by a solution of the full Navier-Stokes equations are in an early stage of development and have not yet become of practical use.

Several calculative techniques have been developed based on patching together approximate models of the flow in the various regions. All of the methods to be discussed herein apply to axisymmetric bodies at zero angle of attack. Presz[1] represents the separated region by a discriminating streamline which modifies the shape of the body upon which a boundary layer is calculated. Control volume analyses locate the separation point and determine the shape of the discriminating streamline. Exhaust plume entrainment is modeled using an integral approach wherein the mixing layer is treated in the same manner as a boundary layer. The technique was found to give good results for Mach numbers less than that for the onset of shock-induced separation, typically a freestream Mach number of about 0.9. Another

approach was taken by Cosner[2] who applies an integral boundary-layer method to the entire body, including the separated region, using empirical relations to extend the calculations across the separation and reattachment points for bodies with solid plume simulators. Exhaust plume entrainment was calculated by simply extending the boundary-layer analysis to the plume boundary treated as a moving wall. The method was not successful for bodies with extensive separation. The most sophisticated approach to the problem of exhaust plume entrainment is that of Dash and Pergament[3] wherein finite-difference methods are used for the flow calculations in all regions of the flow. Separated flow on the nozzle boattail is not considered. However, studies described by Wilmoth[4] indicate that the method correctly accounts for entrainment.

In this paper, a method is described which combines a finite-difference inviscid flow method with integral methods for the boundary-layer and exhaust plume mixing layer. The method uses insights from the previous methods to establish first approximations which are subsequently refined by iteration.

The basic principle of the viscous-inviscid interaction calculation is to define a displacement surface for the viscous layer which forms an effective boundary for the inviscid flow and which is compatible with the resulting inviscid pressure distribution. When the boundary layer is separated, a special iterative technique is used to determine the appropriate viscous flow solution.

Since the principle of the viscous-inviscid interaction is the same whether a sting or a plume exists downstream of the body, the elements of the caculative method will be described in the following order: First, the overall viscous-inviscid interaction method will be described in order to provide a framework for explaining the various individual components of the method. Next, the methods used to calculate the external inviscid flow, the inviscid exhaust plume flow, and the boundary-layer calculative method will be presented, followed by the exhaust plume entrainment model. Finally, some comparisons with experimental data are shown, illustrating the capabilities of the method. The details of the derivations of the calculative methods are presented in Ref. 5.

Viscous-Inviscid Interaction Method

It is well known that for both laminar and turbulent boundary layers, the usual boundary-layer equations exhibit singular behavior at the point of zero skin friction when the pressure gradient is prescribed. The details of the method used to avoid this singular behavior will be described subsequently, along with the description of the integral boundary-layer method. For the present discussion, it is sufficient to note that a method is available for calculating a smooth surface which represents the displacement effect of the boundary-layer, or exhaust plume entrainment layer, including boundary-layer separation.

Estimation of Boundary of Separated Region

The first step in calculating the viscous-inviscid interaction is to calculate the inviscid flow over the basic body. The resulting distribution of the velocity at the boundary is then prescribed in the second iteration step as the boundary-layer-edge velocity u_e for the boundary-layer calculation up to the separation point. A first approximation to the separation point location x_s is obtained by a method which will be described subsequently along with the detailed description of the boundary-layer method. The boundary-layer calculation is carried on into the separated flow using a prescribed distribution of the boundary-layer displacement thickness δ^*. The result of that calculation is a solution for the boundary-layer-edge velocity (the "viscous velocity") which may or may not agree with the "invisicd velocity" produced by the inviscid flow theory. The effective displacement surface between separation and a point downstream of reattachment or in the plume entrainment region is assumed to be conical (Fig. 1). An iterative procedure is used to find the particular cone angle θ_s and separation point location x_s for which the "viscous velocity" and the "inviscid velocity" agree. Downstream of x_p, which will be defined subsequently, the boundary-layer-edge velocity is again prescribed on the viscous flow calculation as the inviscid boundary velocity from the previous calculation. The value of x_p comes from the boundary-layer calculation and therefore may vary at each step of the iteration.

Iteration Procedure

Starting from estimated values of x_s and θ_s, the iteration procedure consists of two cycles (Fig. 2). In the inner cycle, the inviscid flow and the boundary layer are calculated alternately until the largest change in the δ^* solution between iterations becomes smaller than a specified tolerance, and, simultaneously, the inviscid calculation procedure also converges to a specified tolerance. At each step of the cycle, the boundary-layer displacement thickness is used to calculate an augmented body shape by the relation

$$r_n = r_w + \tfrac{1}{2}(\delta_n^* + \delta_{n-1}^*) \tag{1}$$

where r_n is the effective body radius at iteration n.

When the inner cycle has been terminated, if separation is present, the squared deviation between the two velocity solutions between x_s and x_p is calculated. The accuracy of the matching of the two solutions is then indicated by the value of the rms error s where

$$s = \left[\sum_{1}^{N} \frac{(u_{e_V} - u_{e_I})^2}{u_{e_0}^2 N}\right]^{1/2} \tag{2}$$

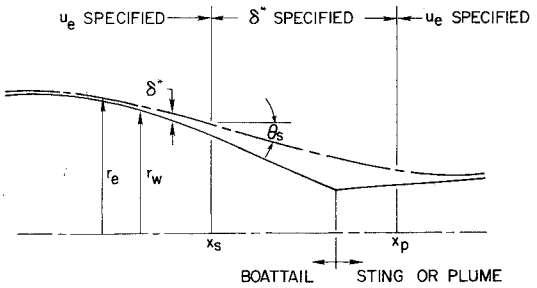

Fig. 1 Effective body shape for separated flow.

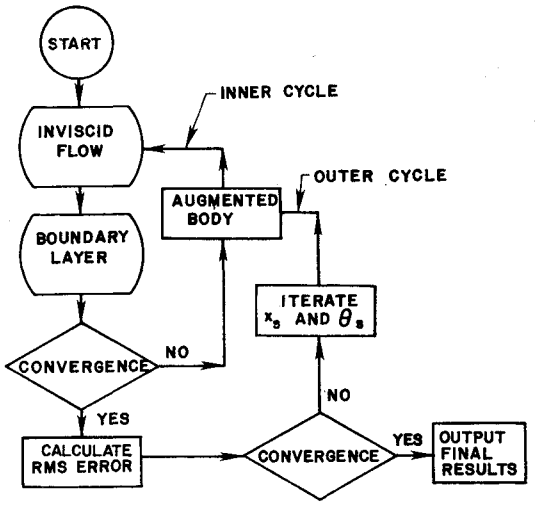

Fig. 2 Iteration cycles.

This quantity is then compared with the value from the previous iteration and if a minimum has not been found, x_s and θ_s are adjusted. The boundary layer is recalculated using the new values of x_s and θ_s, and the calculation re-enters the inner cycle (Fig. 2).

The manner of adjusting x_s and θ_s is as follows: The first value of s [Eq. (2)] is calculated using the estimated values of x_s and θ_s. The next step is to change θ_s a small amount and calculate a second value of s. The third step is to change x_s a small amount, keeping θ_s at the original value, to calculate a third value of s. With these three solutions, the gradient of s with respect to x_s and θ_s is calculated from

$$s_\theta = \frac{\partial s}{\partial \theta_s} = \frac{s_2 - s_1}{\Delta \theta_s} \tag{3}$$

$$s_x = \frac{\partial s}{\partial x_s} = \frac{s_3 - s_1}{\Delta x_s} \tag{4}$$

The maximum rate of decrease of s with respect to x_s and θ_s is in the direction of the negative of the gradient. Therefore, after the third iteration, both quantities are adjusted along the direction of the negative gradient until either a specified tolerance is met or a minimum value of s is reached. If a minimum is found without satisfying the tolerance, the sequence is restarted, calculating a new gradient direction. If this procedure does not produce a value of s less than the specified tolerance after four restarts, the sequence is terminated.

A third element in the iteration procedure is the calculation of the inviscid exhaust plume. The entrainment of the boundary-layer flow and the turbulent mixing between the external inviscid flow and the exhaust plume flow are assumed to take place along a boundary defined by the radius the exhaust plume would have with all mixing neglected. This "inviscid reference surface" is calculated twice during the iteration process described previously. The first plume calculation is performed assuming an external flow parallel to the jet axis with constant pressure and the freestream Mach number. After four cycles of the iteration, a new exhaust plume is calculated using the external pressure distribution that exists at that time as calculated by the inviscid theory. Tests in which the plume was calculated a third time using the final converged pressure distribution indicated that only a slight change in the plume occurred. The effect on the flow characteristics on the body was small. Thus, the solution is not sensitive to small deviations from the exact shape of the jet mixing boundary.

Inviscid Flow Model

The inviscid flow method employed herein is the method of South and Jameson described in Ref. 6. The computer program used is that described in Ref. 7 with minor modifications to accommodate the iteration between the inviscid and viscous flows. With this method, the entire subsonic and transonic velocity range can be calculated, and slightly supersonic freestream Mach numbers are permissible as long as entropy production by shock waves is negligible.,

Inviscid Plume Model

The inviscid exhaust flow calculation method used in this work is the same as the Henson-Robertson shock-expansion/one-dimensional method (Ref. 8) with two exceptions:

1) Compressions are computed as reverse Prandtl-Meyer expansions rather than by means of Newtonian impact theory.

2) Flow areas are computed as plane areas normal to the nozzle centerline rather than as spherical areas.

The plume shape is calculated in a series of straight-line segments which approximate the curved shape of the plume. The external pressure is compared with the internal pressure at the exit plume boundary point and at each consecutive boundary point, and an expansion or compression turn is calculated depending on the comparison.

The plume boundary velocity q_p corresponding to each axial station is computed from isentropic relations with the specified nozzle stagnation conditions. In order to approximate the velocity distribution in each cross section of the plume, the flow is assumed to be locally source-like, so that the velocity components u_c and v_c required at r_c, the inner boundary of the turbulent mixing layer, are approximated by

$$u_c = q_p \left[1 + \left(\frac{r_c}{r_w} \frac{dr_w}{dx} \right)^2 \right]^{-1/2} \tag{5}$$

$$v_c = u_c \frac{r_c}{r_w} \frac{dr_w}{dx} \tag{6}$$

Development of Boundary-Layer Method

The complete derivation of the governing equations for the boundary layer has been presented in Ref. 9. In this report the equations as modified in Ref. 5 for the application of interest herein are summarized.

Boundary-Layer Equations for Compressible Turbulent Flow

The basic notation and coordinate scheme are shown in Fig. 3. It is noted that these coordinates are not the usual boundary-layer coordinates. They are employed to avoid difficulties at sharp concave corners such as a boattail-sting junction.

The governing equations describing the steady flow of a compressible turbulent boundary layer in these coordinates are:

$$(r\rho u)_x + \{r\rho[v - (r_w)_x u]\}_y = 0 \tag{7}$$

$$\rho u u_x + \rho[v - (r_w)_x u] u_y = -p_x + (1/r)(r\mu\beta u_y)_y \tag{8}$$

$$\rho u S_x + \rho[v - (r_w)_x u] S_y = (1/r)(r\mu\beta S_y)_y \tag{9}$$

Transformation of the Boundary-Layer Equations

Applying the Probstein-Elliott transformation[10] and the Stewartson transformation,[11] along with the assumptions that the viscosity varies linearly with the temperatures and laminar and turbulent Prandtl numbers are unity, reduces the equations of the boundary layer to those of a two-dimensional, incompressible boundary layer.

The solution of the transformed energy equation is approximated by the relation

$$S = S_w (1 - U/U_e) \tag{10}$$

The density profiles are then related to the velocity profiles through the temperature.

$$(\rho_e/\rho) = (T/T_e) = (S+1)(1+m_e) - m_e (u/u_e)^2 \tag{11}$$

Thus, the velocity profiles found to be valid for incompressible, two-dimensional turbulent boundary layers can be used by simply transforming the input quantities to the incompressible plane, performing the calculation for an equivalent incompressible boundary layer, and then transforming the results back to the compressible flow in axisymmetric coordinates.

Development of Integral Boundary-Layer Method

Integral Equations

The integral method used herein was described in detail in Ref. 12. Integral equations are derived by eliminating the transformed normal velocity V between the transformed

momentum and continuity equations and then taking weighted integrals of the resulting equation across the boundary layer. The result is two equations

$$\int_0^{\delta_i} \left\{ UU_X - U_Y \int_0^Y U_X \mathrm{d}\eta - (S+1)U_e(U_e)_X - C\nu_{e_0}[(1+t\tilde{y})U_Y]_Y \right\} Y^n \mathrm{d}Y = 0 \quad (12)$$

with $n=0$ and 1.

Velocity Profiles

The velocity profiles are represented by the function

$$U = U_\tau [2.5\ell n(1+Y^+) + 5.1 - (3.39Y^+ + 5.1)\exp(-0.37Y^+)] + U_\beta \sin^2 \frac{\pi}{2}\frac{Y}{\delta_i} \quad (13)$$

with

$$U_\tau = (C_f/|C_f|)U_e\sqrt{|C_f|/2} \quad (14)$$

The variable Y^+ is defined to account for the axisymmetry of the flow

$$Y^+ = (L/r_w)(|U_\tau| Y/\nu_{e_0}) \quad (15)$$

The exponential terms in Eq. (13) and the additional unit in the logarithmic term provide a smooth transition from the turbulent flow to the wall through a laminar sublayer.

Eddy Viscosity

The eddy viscosity model used in this work is a two-layer model using Clauser's expression with intermittency for the outer layer and a modification of the outer layer for adverse pressure gradients and separated flows. In the inner layer of attached flows, the eddy viscosity parameter β is represented by an exponential expression based on the law of the wall. For separated flows, the scaling of the outer eddy viscosity is a displacement thickness based on the velocity profile above the $U=0$ line. Transition from laminar to turbulent flow is calculated by letting the eddy viscosity change from a laminar viscosity to a fully turbulent value over a short distance.

Equations Solved

Substitution of Eq. (13) into the two equations derived from Eq. (12) produces two ordinary differential equations for the variation of the variables $U_\tau, U_\beta, \delta_i$, and U_e with x. A third equation produced by evaluating Eq. (13) at $Y=\delta_i$ allows the elimination of U_β from the equations, leaving a set of two equations

$$A_{n1}(U_\tau)_x + A_{n2}\delta_{i_x} + A_{n3}(U_e)_x = B_n \quad (16)$$

with $n=1$ and 2, where the coefficients are integral functions of U_τ, δ_i, and U_e. These integrals are evaluated numerically, using a simple 11-point trapezoidal integration.

The usual procedure for solving Eq. (16) for attached boundary layers is to prescribe the pressure distribution or the boundary-layer-edge velocity distribution U_e. However, if separation occurs, the pressure distribution cannot be prescribed arbitrarily in the separated region. If an adverse pressure gradient is prescribed for an attached boundary layer, the value of U_τ can approach zero. When U_τ vanishes, the coefficients A_{11} and A_{21} in Eq. (16) also vanish, producing a singularity. The singularity is removed by expressing the displacement thickness δ^* in terms of U_τ, δ_i, and U_e through the definition

$$\delta^* = \int_0^\delta (1-\rho u/\rho_e u_e)(r/r_w)\mathrm{d}y \quad (17)$$

The result is differentiated with respect to x, producing a third equation,

$$A_{31}(U_\tau)_x + A_{32}\delta_{i_x} + A_{33}(U_e)_x + A_{34}\delta^*_x = B_3 \quad (18)$$

where the A_{3j} and B_3 are functions of U_τ, δ_i, and U_e.

Like the coefficients A_{11} and A_{21}, the coefficient A_{31} also vanishes when $U_\tau = 0$. However, it can be shown that A_{11}/A_{31} and A_{21}/A_{31} are both finite when $U_\tau = 0$. This allows the three equations, Eq. (16) with $n=1$ and 2 and Eq. (18), to be reduced to two ordinary differential equations in the three dependent variables—δ^*_x, δ_{i_x}, and $(U_e)_x$—by eliminating the $(U_\tau)_x$ terms. The differential equations are then solved with a prescribed variation of δ^*. The value of U_τ is then obtained directly from known values of δ_i, δ^*, and U_e by solving the nonlinear relation, Eq. (17).

Method of Solution of Equations

The equations to be solved are integrated numerically using the elementary predictor-corrector scheme described by Nash and Hicks,[13] with an integration step Δx taken to be 1/8 of each finite-difference step of the inviscid calculational mesh. This provides a fast, accurate method of solution.

Calculation of Separated Boundary Layers

It is well known that for both laminar and turbulent boundary layers, the usual boundary-layer equations exhibit singular behavior at the point of zero skin friction when the pressure is prescribed (or, equivalently, when the boundary-layer-edge velocity is prescribed). A recent development used to avoid the singularity is the use of an inverse technique in which the pressure or the boundary-layer-edge velocity is calculated and some other quantity such as δ^* is prescribed. However, the flow near the separation point may still require special treatment, even with the singularity removed. It has been observed by many authors (c.f. Cebeci et al.,[14] and Gerhart and Bober[15]) that the use of the experimental pressure distribution from a separated flow in a solution of the boundary-layer equations does not always produce a singularity. Often the calculated skin friction will simply decrease to some minimum value and then increase, with the calculated boundary layer remaining attached in a region known from experiment to be separated. The reason for this is believed to be due to the neglect of the terms in the Navier-Stokes equations which respond to downstream perturbations, i.e., the normal stress terms and normal pressure gradient terms. On the other hand, the work of Newman[16] and Simpson[17] has shown that these terms are negligible a short distance away from separation, even though they can be very significant in the immediate vicinity of the separation point.

The approach taken in the present work is an engineering approximation based on the following assumptions:

1) Upstream influences are transmitted predominantly through the external inviscid flow which is elliptical in nature for a locally subsonic flow.

2) Violations of the boundary-layer assumptions, such as significant normal pressure gradients associated with separation, can be neglected on the grounds that they are only important in a small neighborhood of the separation point and have negligible effect on the rest of the flow.

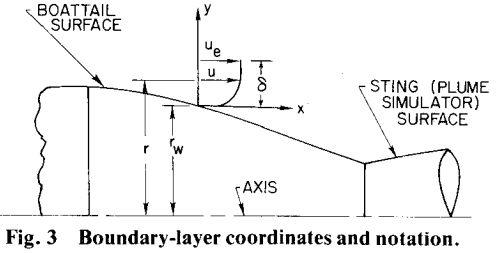

Fig. 3 Boundary-layer coordinates and notation.

In the apprach taken herein, the location of the separation point is obtained independently from the boundary-layer calculation, and the skin friction is specified to be zero at that point, keeping the boundary-layer-edge velocity and the displacement thickness δ^* continuous. This means that the variation of C_f upstream of the separation point is slightly in error—the amount depending upon the extent of the neglected upstream influence.

A first approximation to the location of separation x_s is found by computing the shape factor H_i

$$H_i = \int_0^{\delta_i} (1-U/U_e)\,dy \Big/ \int_0^{\delta_i} U/U_e(1-U/U_e)\,dy \qquad (19)$$

For the velocity profiles given by Eq. (13), this parameter has a value of 4.0 when $U_\tau = 0$. However, experimental measurements indicate that separation actually occurs when H_i is approximately 2.0. This suggests that the present boundary-layer formulation is not accurate in the vicinity of the separation point. This is not unexpected in light of the previous discussion. Also, the velocity profiles of Eq. (13) have been demonstrated to provide a reasonable approximation to both attached and separated boundary layers,[18] but to be of questionable accuracy at the point of zero skin friction. However, the effect of this inaccuracy is believed to be confined to the immediate vicinity of the separation point for the kind of flows of interest here. Accordingly, the first approximation to the value of x_s is taken to be the location at which H_i equals a specified value for the inviscid velocity calculated for the basic body.

When a value of x_s is established, the boundary layer is calculated from the nose of the body to x_s with the distribution of u_e from the external inviscid flow calculation prescribed using Eqs. (16). At x_s, the velocity u_e and the displacement thickness δ^* are assumed to be continuous (see Fig. 4). The friction velocity U_τ on the other hand, is assumed to be zero as the initial value for the integration into the separated region with δ^* prescribed. It must be noted that the calculation could be started with a positive value of U_τ and the calculation would proceed through the point where $U_\tau = 0$ for an appropriate δ^* distribution with no singularity. However, due to the approximations inherent in the theory in the vicinity of the separation point, as discussed previously, it is not possible to determine the correct positive values of U_τ approaching separation.

At some point after reattachment, the calculation procedure must be changed back to the u_e prescribed mode using Eqs. (16). The determination of the point x_p for this switch is based on the behavior of the velocity u_e produced by the boundary-layer solution. As shown in Fig. 4, u_e becomes nearly constant in the increasing δ^* region between x_s and the end of the body. Then, as the boundary layer proceeds toward reattachment, u_e decreases, eventually reaching a minimum a short distance downstream of reattachment. The minimum point is designated as x_p, and the solution is switched back to the u_e prescribed mode. When x_p is reached, there is not an exact match between u_{eV} and u_{eI}. A linear transition is prescribed from the current value of u_{eV} to the value of u_{eI} at the second external flow computational grid station downstream of x_p, or at the first subsequent point at which $u_{eI} > u_{eV}$. The overall iteration procedure does not appear to be very sensitive to this transition since u_{eV} approaches u_{eI} as the solution converges.

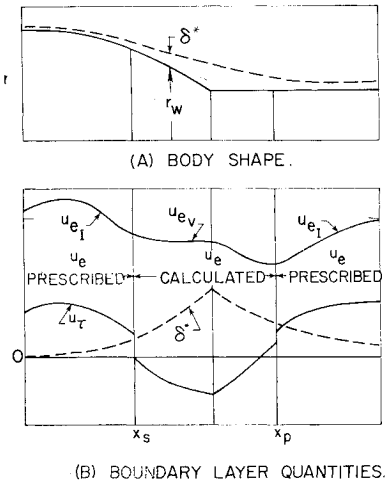

Fig. 4 Separated flow quantities (schematic).

Exhaust Plume Entrainment Model

The flowfield of an exhaust jet mixing with a subsonic external flow and a separated boattail boundary layer is shown in Fig. 5. Two regions can be distinguished in the flowfield. In region 1, the boundary layer merges with the mixing layer at the exhaust plume boundary and the exhaust plume contains a core of inviscid core flow. In region 2, the turbulent mixing reaches all the way to the axis of the jet so there is no inviscid core flow. In this report, only the flow in region 1 is considered since for the kinds of flow conditions of interest, the entrainment is expected to be essentially completed in the length of the inviscid core. The effective boundary of the jet is assumed to be cylindrical downstream of the inviscid core.

Equations for Mixing Layer

The mixing layer is assumed to develop about a surface defined by the radius the plume would have if it was completely inviscid and subject to the pressure distribution calculated from the external inviscid flow. The basic equations are assumed to be the same as those of a turbulent boundary layer. In cylindrical coordinates for axisymmetric flow, these equations have been presented previously as Eqs. (7-9). For the entrainment layer, as for the boundary layer, the energy equation [Eq. (9)] is approximated by an assumed temperature-velocity relation.

Development of Integral Method for the Mixing Layer

Integral Equations

For the entrainment layer, two equations are derived by eliminating the radial velocity terms between the continuity and momentum Eqs. (7) and (8) and integrating the resulting equation across the mixing layer in two strips. No compressibility or geometric transformations are used. Eliminating the $[v-u(r_w)_x]$ term between the momentum and continuity equations and integrating yields

$$\int_{r_c}^{r} \rho u r u_x\,dr - \int_{r_c}^{r} u_r \int_{r_c}^{\eta} (\rho u r)_x\,d\eta\,dr = r\mu\beta u_r$$
$$- \tfrac{1}{2}(r^2 - r_c^2)p_x - \rho_c r_c[v_c - u_c(r_w)_x](u-u_c) \qquad (20)$$

where it has been assumed that the shear stress term vanishes at r_c, the inner boundary of the mixing layer. Evaluating Eq.

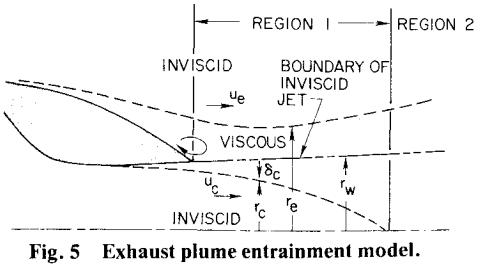

Fig. 5 Exhaust plume entrainment model.

(20) at $r=r_w$ and $r=r_e$ yields two independent integral equations.

For the boundary layer, the effective shape required for the viscous-inviscid interaction is defined by the body radius plus the boundary-layer displacement thickness, Eq. (17). In a similar manner, a displacement thickness is defined for the exhaust jet. For purely inviscid flow, the boundary of the exhaust jet is a streamline separating the nozzle efflux from the external flow. With entrainment and turbulent mixing, this line is no longer a streamline. However, in order to produce a continuous and smooth surface for the external inviscid flow, it is postulated that the effective boundary may be defined by a displacement from the inviscid plume boundary in the same manner as for a solid boundary. Thus, an additional equation is derived by defining

$$\delta^* = \int_{r_w}^{r_e} (1-\rho u/\rho_e u_e)\,(r/r_w)\,dr \tag{21}$$

where r_w is now the radius of the inviscid plume boundary.

Velocity Profiles

The flow profiles of the mixing layer are assumed to be composed of a linear combination of functions representing the boundary-layer profile at the nozzle exit and the self-similar profiles of an equilibrium jet boundary profile far downstream. Thus,

$$u=(1-K)u_n+Ku_s \tag{22}$$

where u_n is a velocity profile proportional to the boundary-layer profile at the nozzle exit station (including both internal and external boundary layers), u_s is a velocity profile function representing the downstream profile, and K is a factor to be determined.

A family of profiles of u is shown for illustration in Fig. 6. The similarity behavior of the downstream profile is assumed to be approximated by a sine function. These definitions contain five quantities which must be determined to describe the flow. Two of the required quantities, r_w and u_c, are determined by the approximate model of the flow in the inviscid exhaust jet. The remaining three quantities, u_e, δ_c, and K, are calculated from solutions of the equations derived from Eqs. (20) and (21), combined with the inviscid external flow in the same manner as described previously for boundary layers.

Temperature-Velocity Relationship

A transitional model of the temperature profile is defined as

$$S=(1-K)S_n+KS_s \tag{23}$$

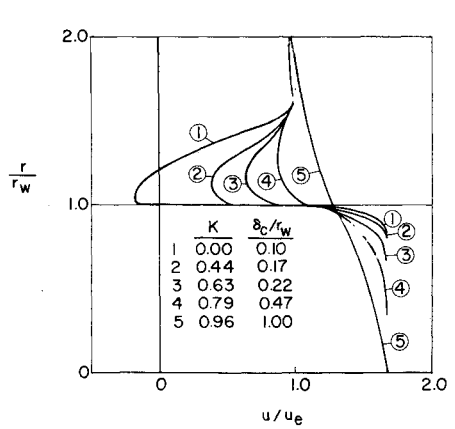

Fig. 6 Typical entrainment region velocity profiles.

where, for $r>r_w$,

$$S_n=[1-(u/u_e)]S_w \tag{24}$$

and for $r<r_w$,

$$S_n=[1-(u/u_c)]S_w+S_c(u/u_c) \tag{25}$$

and

$$S_s=S_c\frac{u_s-u_e}{u_c-u_e} \tag{26}$$

The density profiles are related to velocity profiles through the temperature by Eq. (11) in the same way as for the boundary layer.

Turbulent Shear Stress

In Eq. (20) it has been assumed that the shear stress is related to the radial velocity gradient through an eddy viscosity in the same manner as for the boundary layer on the body. In the integral equations, only the value of the shear at the boundary $r=r_w$ is needed.

As for the velocity and temperature profiles, the eddy viscosity for a shear layer, such as the jet boundary far downstream of the nozzle, is found in the literature to have a specific form different from that of the boundary layer. In the present work, the eddy viscosity was assumed to undergo a transition from the value on the body to a value determined for the downstream flow in the same manner as for the velocity and temperature profiles, so that

$$\beta=-K+\frac{0.018K}{\nu_{e_0}}\left[\left(\frac{1+m_e}{1+m_c}\right)\left|\frac{u_c+u_e}{u_c-u_e}\right|\right]^{0.9}\delta_c\,|u_c-u_e| \tag{27}$$

Equations Solved

The equations to be solved are[5]:

$$A_{n1}K_x+A_{n2}(\delta_c)_x+A_{n3}(u_e)_x=B_n \quad \text{with } n=1,2, \text{ or } 3 \tag{28}$$

The first two of these equations are the momentum integral equations from Eq. (20) evaluated at r_w and r_e, and the third equation is the derivative of Eq. (21). A similar approach is taken to solving the entrainment equations as was used for the boundary-layer equations. At the end of the body (the beginning of the entrainment region), the value of δ^* is known, along with r_e and u_e. A value of δ_c is determined from a nozzle boundary-layer calculation. The value of K is assumed to be zero. The variation of δ^* is specified continuously from the boundary layer into the entrainment region, while u_e, δ_c, and K are calculated by solving Eq. (28). To accomplish this calculation, the first two of Eqs. (28) are reduced to two equations in $(\delta_c)_x$ and $(u_e)_x$ by eliminating K_x with the third equation. The value of K is then determined by solving Eq. (21) directly. When the point of minimum u_e is reached downstream of the nozzle, u_e is prescribed as for the boundary layer on a sting and the values of K and δ_c are calculated from the first two of Eqs. (28).

Results

In this section, the theory is compared with experimental results on axisymmetric boattail-sting and boattail-exhaust plume configurations. In all cases, the boundary layer was initiated as a laminar boundary layer near the nose of the forebody with transition specified shortly downstream of the initial point.

Circular Arc Boattails with Solid Plume Simulators

Comparisons between the theory and measured results from Ref. 19 for the pressure distributions on a circular arc boattail at $M_0=0.6$, 0.8, and 0.9 are presented in Fig. 7. The configuration forebody is a cone cylinder with boundary-layer transition tripped at $x/D=0.167$. For the two lowest Mach numbers, the theory is seen to be in excellent agreement with

the data on the boattail, with a slight discrepancy on the solid plume simulator. Also, the calculated location of the separation point agrees exactly with that determined by oil flow[20] for the $M_0 = 0.6$ case with a small error noted for the $M_0 = 0.8$ case. For the $M_0 = 0.9$ case, the agreement is not as good. A fairly large discrepancy is noted in the pressure coefficient over the entire boattail, and a larger error occurs in the prediction of the separation location. For that case, supersonic flow occurs over the beginning of the boattail, with a shock of Mach number approximately 1.25 just ahead of the separation point. Abeyounis[20] suggests that for this configuration, the separation for freestream Mach numbers above 0.8 probably occurs at the shock. Thus, the discrepancies noted in Fig. 7 for $M_0 = 0.9$ probably exist because the present theoretical model assumes separation occurs behind the shock. Another measure of the accuracy of the solution is the degree of convergence of the calculated viscous-inviscid interaction. For the calculations for $M_0 = 0.6$ and 0.8, the iteration converged to an rms error of 1.0%, while the results shown for $M_0 = 0.9$ had an rms error of 2.3%.

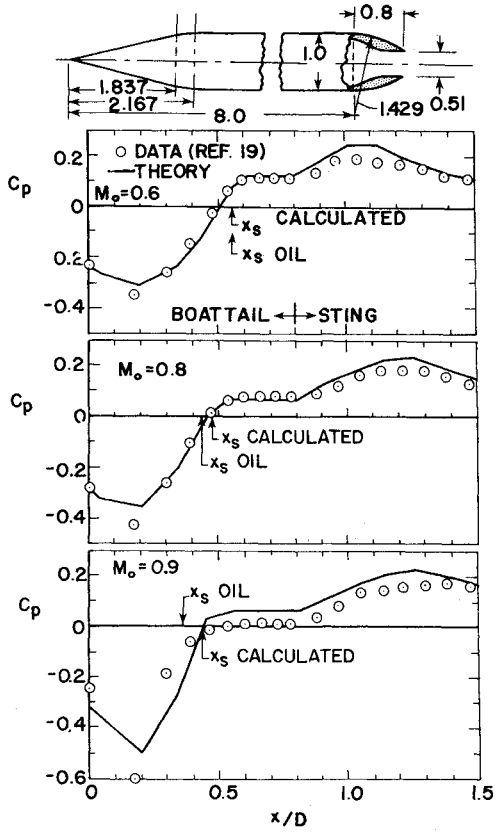

Fig. 7 Comparison of calculated and measured pressure coefficient distributions on boattails with solid plume simulators.

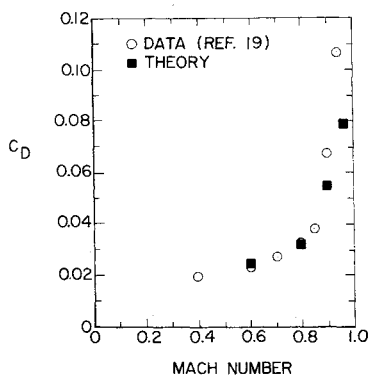

Fig. 8 Comparison of calculated and experimental integrated pressure drag coefficients on boattails with solid plume simulators.

The integrated pressure drag on the boattail is shown in Fig. 8. The calculated values at $M_0 = 0.6$ and 0.8 are in excellent agreement with the data for the separated flow. For higher Mach numbers, the agreement is not as good, as would be expected from the pressure coefficient comparisons and the previous discussion. Even, so the calculations for $M_0 = 0.9$ and an additional calculation at $M_0 = 0.96$ indicate the method predicts the transonic drag rise with fair accuracy.

Circular Arc Boattails with Compressed Air Plumes

Some of the wind tunnel tests of Ref. 19 were conducted with the exhaust plume simulated with high-pressure air. Comparisons between the theory and data for the pressure coefficient distributions on the boattail are presented in Fig. 9 for exhaust nozzle total pressure ratios of 2.0 and 4.0 at a freestream Mach number of 0.8. The agreement between the theory and data for a pressure ratio of 2.0 is good even though there is some error in the predicted separation point location.

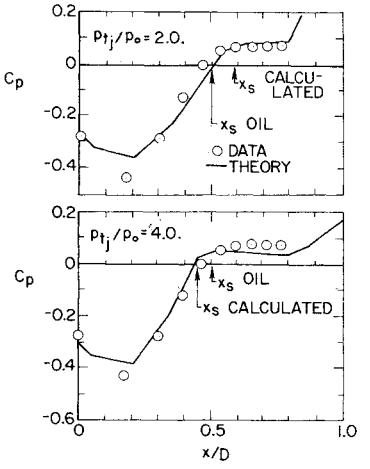

Fig. 9 Comparison of calculated and measured pressure coefficient distributions with high-pressure air plume, $M_0 = 0.8$.

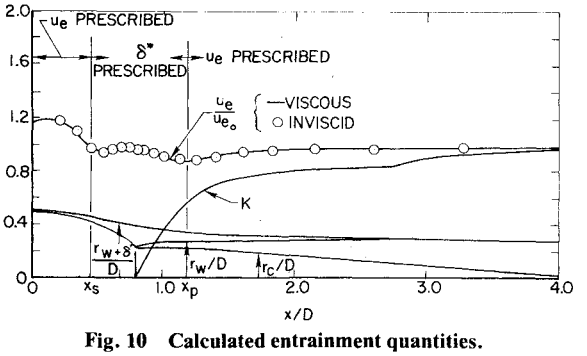

Fig. 10 Calculated entrainment quantities.

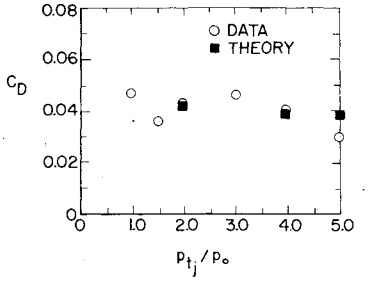

Fig. 11 Comparison of experimental and calculated boattail drag with high-pressure air plume, $M_0 = 0.8$.

The comparison for a nozzle pressure ratio of 4.0 indicates good agreement for the pressure coefficient distribution and somewhat better agreement for the separation point location than the previous case. The rms errors of the calculations were 1.6% and 1.1%, respectively.

Plots of the important entrainment region parameters are presented in Fig. 10 for the case with exhaust total pressure ratio of 4.0. The plume inviscid reference surface represented by r_w is seen to expand slightly as it leaves the nozzle, reaching an essentially cylindrical shape in approximately two nozzle diameters. The inner boundary of the mixing region, represented by r_c, requires more than six nozzle diameters to reach the axis of the plume. The entrainment parameter K increases rapidly at first and then more gradually after x_p is reached and the calculation switches from prescribed δ^* to prescribed u_e. The entrainment reaches completion ($K=1.0$) asymptotically, but is effectively complete in less than six nozzle diameters.

Boattail drag coefficients calculated from the measured and calculated pressure coefficient distributions of Fig. 9 are shown in Fig. 11. The theoretical drag coefficients for the pressure ratios of 2.0 and 4.0 are in excellent agreement with the data. A third case, for an exhaust total pressure ratio of 5.0, has a calculated drag coefficient slightly higher than the data. The rms error for the case was 3.2%.

It is noted that additional comparisons shown in Ref. 5 indicate that the present jet entrainment model is more accurate for moderately underexpanded plumes as shown herein. For low-pressure exhaust jets, or highly underexpanded plumes, the iteration procedure is somewhat sensitive to the initial conditions. This is believed to be due in part to the approximate nature of the present entrainment model and to the inaccuracy of the conical approximation of the effective body shape in the entrainment region. An improved entrainment model and a better approximation of the body shape are under development.

Conclusions

The calculative method has been found to be applicable to both attached and separated flows on boattails with solid plume simulators and with high-pressure jets. Comparisons with experimental data indicate that the entrainment model and the viscous-inviscid iteration procedure provide an accurate engineering method for predicting boattail flowfields for moderately underexpanded exhaust flows and for boattails with solid exhaust plume simulators.

Acknowledgments

This work was sponsored by the Arnold Engineering Development Center, Air Force Systems Command, USAF under Contract No. F40600-77-C-0008.

References

[1] Presz, W. M., Jr., King, R. W., and Buteau, J. D., "An Improved Analytical Model of the Separation Region on Boattail Nozzles at Subsonic Speeds," NASA CR-3028, July 1978.

[2] Cosner, R. R. and Bower, W. W., "A Patched Solution of the Transonic Flow Fields About an Axisymmetric Boattail," AIAA Paper 77-227, Los Angeles, Calif., Jan. 1977.

[3] Dash, S. M. and Pergament, H. S., "A Computational Model for the Prediction of Jet Entrainment in the Vicinity of Nozzle Boattails (The BOAT Code)," NASA CR-3075, Aug. 1978.

[4] Wilmoth, R. G., Dash, S. M., and Pergament, H. S., "A Numerical Study of Jet Entrainment Effects on the Subsonic Flow Over Nozzle Afterbodies," AIAA Paper 79-0135, New Orleans, La., Jan. 1979.

[5] Kuhn G. D., "Computer Program for Calculation of Separated Turbulent Flows on Axisymmetric Afterbodies Including Exhaust Plume Effects," AEDC TR-79-4, March 1979.

[6] South, J. C., Jr. and Jameson, A., "Relaxation Solutions for Inviscid Axisymmetric Transonic Flow Over Blunt or Pointed Bodies," *AIAA Computational Fluid Dynamics Conference Proceedings*, Palm Springs, Calif., July 19-20, 1973.

[7] Keller, J. D. and South, J. C., Jr., RAXBOD: A FORTRAN Program for Inviscid Transonic Flow Over Axisymmetric Bodies," NASA TM X-72831, Feb. 1976.

[8] Henson, J. R. and Robertson, J. E., "Methods of Approximating Jet Boundaries for Highly Underexpanded Supersonic Nozzles," AEDC TDR-TR 62-7, May 1962.

[9] Kuhn, G. D., "Calculation of Compressible, Nonadiabatic Boundary Layers in Laminar, Transitional and Turbulent Flow by the Method of Integral Relations," NASA CR-1797, Nov. 1971.

[10] Probstein, R. F. and Elliott, D., "The Transverse Curvature Effect in Compressible Axially Symmetric Laminar Boundary-Layer Flow," *Journal of the Aeronautical Sciences*, Vol. 23, 1956, p. 208.

[11] Stewartson, K., "Correlated Incompressible and Compressible Boundary Layers," *Proceedings of the Royal Society, A*, Vol. 200, 1949, pp. 85-100.

[12] Kuhn, G. D. and Nielsen, J. N., "An Analytical Method for Calculating Turbulent Separated Flow Due to Adverse Pressure Gradients," Project SQUID Tech. Rept. NEAR-1-PU, Oct. 1971.

[13] Nash, J. F. and Hicks, J. G., "An Integral Method Including the Effect of Upstream History on the Turbulent Shear Stress," *Proceedings of the 1968 AFOSR-IFP-Stanford Conference on Computation of Turbulent Boundary Layers,* Stanford University, Calif., p. 41.

[14] Cebeci, T., Mosinskis, G., and Smith, A.M.O., "Calculation of Separation Points in Incompressible Turbulent Flows," *Journal of Aircraft*, Vol. 9, Sept. 1972, pp. 618-624.

[15] Gerhart, P. and Bober, L., "Comparison of Several Methods for Predicting Separation in a Compressible Turbulent Boundary Layer," NASA TM X-3102, 1974.

[16] Newman, B. G., "Some Contributions to the Study of the Turbulent Boundary Layer Near Separation," Australian Dept. of Supply, Rept. ACA-53, March 1951.

[17] Simpson, R. L., "Characteristics of a Separating Incompressible Turbulent Boundary Layer," Paper No. 14 in *Flow Separation*, AGARD CP-168, May 1975.

[18] Alber, I. E., Bacon, J. M., Masson, B. S., and Collins, D. J., "An Experimental Investigation of Turbulent Transonic Viscous-Inviscid Interactions," *AIAA Journal*, Vol. 11, May 1973, pp. 620-627.

[19] Reubush, D. E., "Experimental Study of the Effectiveness of Cylindrical Plume Simulators for Predicting Jet-On Boattail Drag at Mach Numbers Up to 1.3," NASA TN D-7795, Nov. 1974.

[20] Abeyounis, W. K., "Boundary Layer Separation on Isolated Boattail Nozzles," M.S. Thesis, School of Engineering and Applied Science, The George Washington University, May 1977.